Journal of Structural Geology, Vol. 10, No. 4, pp. 413 to 430, 1988
Printed in Great Britain

0191-8141/88 $03.00 + 0.00

On the formation and growth of faults: an experimental study

S. J. D. Cox* and C. H. Scholz

Lamont-Doherty Geological Observatory and Department of Geological Sciences of Columbia University, Palisades, NY 10964, U.S.A.

(*Received* 10 *March* 1987; *accepted in revised form* 14 *January* 1988)

Abstract—By using an experimental geometry, which includes a slot loaded to produce a mode 3 shear stress concentration, shear fractures have been grown in two fine-grained rock types. The deformation is accomplished by initially generating an array of oblique, mainly tensile, cracks at the tip of the slot, which are subsequently linked to form a rupture zone. This suggests a more general model for the formation of brittle shear rupture. A through-going shear surface will form if a damage zone is concentrated enough in the appropriate orientation. This may occur at the edges of an existing shear strain discontinuity, such as a fault, particularly in a mode 3 displacement field. Thus under some conditions faults may grow or link up as true macroscopic shear ruptures. This may be part of a solution to the apparent paradox of the existence of long faults. We suggest features that would indicate this sequence of formation in the field and review some geological examples.

INTRODUCTION

Under the temperatures and pressures present in the upper part of the earth's crust, most of the constituent materials have an elastic–brittle response to stresses. The most significant deformation accommodating structures are faults, which are the brittle form of a shear strain concentration. These can be very long with large amounts of slip concentrated on essentially planar discontinuities.

Early studies of the brittle behavior of materials in the framework of continuum mechanics led to predictions of the orientation of failure surfaces relative to the stress directions (Mohr–Coulomb theory). By applying this on a large scale to faulting in the earth, Anderson (1951) provided a valuable tool in structural geology for constraining the orientations of stress fields. Attempts to rationalize the failure envelope with models of the processes leading to fracture on a micro-mechanical scale have had some success (Brace 1960). However, the genesis of continuous faults has been a source of some discussion: specifically on the displacement mode of the fractures that later become long uniform shear discontinuities.

Simple model experiments by Brace & Bombolakis (1963), Lajtai (1971) and Shamina *et al.* (1975), and on rock by Ingraffea (1981), support the theoretical prediction (Lawn & Wilshaw 1975) that single cracks growing from slots in plates, even loaded to produce large shear-stress concentrations, rapidly reorient to become parallel to the maximum compressive stress. Holzhausen (1978), using a rock-like model material, managed to grow shear cracks a short distance before they turned and the experiments of Laqueche *et al.* (1986) grew shear cracks by taking advantage of the natural fabric in a schist. Taken at face value these experiments imply that short shear cracks cannot normally grow to become long ones, hence there is a major problem in explaining the existence of long faults.

Segall & Pollard (1983) have convincingly shown that extension fractures may be reactivated with shear displacements. However, as a general model of fault formation this is unsatisfactory, since every case of Andersonian faulting would have had to be preceded by an earlier stress field with the orientation appropriate to form the tensile fractures later reactivated in shear, and in the case of a conjugate set, by two. Furthermore, Segall & Pollard (1983) and Segall & Simpson (1986) found that the length of the reactivated joints is quite limited and the total shear displacements very small. For general applicability, the initial tensile fractures would have to be persistent enough to form very long fault systems capable of accommodating the large displacements observed in nature. At moderate depths, in the absence of high-fluid pressures, large lithostatic stresses would tend to resist the dilation required for long tensile crack formation.

At the very least, some form of linking and coalescence of shorter existing flaws must play a major role in the formation of long faults (Brace & Bombolakis 1963, Shamina *et al.* 1975, Horii & Nemat-Nasser 1985). Large faults typically have several strands and considerable roughness that suggest some compound origin (e.g. Knipe & White 1979, Gamond & Giraud 1982, Naylor *et al.* 1986).

Previous experimental studies of fault formation in initially intact samples (e.g. Ohnaka 1973) have used geometries in which it is difficult to observe the micromechanics of rupture propagation, since when samples are retrieved the plane is either already completely formed, or it is unclear exactly where the incipient fracture zone is located. Recent sandbox experiments by Naylor *et al.* (1986) illustrate the growth of a fault from a displacement discontinuity in a granular material. Shamina *et al.* (1975) studied the interaction in plates of

* Present address: CSIRO, Division of Geomechanics, P.O. Box 54, Mt. Waverley, Victoria, 3149, Australia.

alabaster with two parallel slots inclined to the compressive stress direction and found that for certain geometries linkage by shear fracture was possible if the separation between the slots was not too great, and Sobolev (1986) has recently extended this with lubricated glass plates representing the pre-existing fault; but otherwise, where a single initial crack was introduced in rock, it has proved difficult to produce shear fractures in simple cases of in-plane loading.

We have conducted a series of experiments loading samples of rock in a configuration that imposes an extended shear stress concentration. Mechanical data are described in a companion paper (Cox & Scholz in press). We report here on microscopic observations of the rupture zone and discuss the implications for fault formation in the earth.

Table 1. Summary of experimental samples

Sample	Axial load (kN)	Starter notch depth (mm)	Peak torque (Nm)	Final offset (μradians)
Westerly granite				
p12	0	8.6	34	1200
p16	5	8.0	95	900
p17	5	8.0	81	2000
p21	25	8.0	110	900
p22	1	8.0	66	1000
Solnhofen limestone				
s02	0	8.3	32	600
s03	0	7.6	36	1350
s06	0	7.0	42	350
s07	0	7.0	40	400
s17	1	8.0	51	200
s18	2.5	8.0	60	200
s19	2.5	8.0	59	230
s21	5	8.0	73	300

EXPERIMENTAL PROCEDURE

Under the fracture mechanics approach to brittle failure we distinguish three displacement modes at crack tips (Fig. 1a) which may be superposed to form the general case. The edges of cohesionless shear cracks have mode 2 and 3 geometries. The earlier experimental studies had various proportions of combined mode 1 and 2 loading. Here we studied the deformation induced by a pure mode 3 (anti-plane shear) stress concentration. In the earth, large-scale mode 3 stress concentrations (c.f. screw dislocations) would be present at the lateral edges of dip-slip faults, or at the base of a finite depth strike-slip fault, assuming a sufficient reduction in cohesion on the existing fault plane.

Sample configuration

The basic experimental configuration is summarized in Fig. 1(b). Cylindrical samples of rock (Solnhofen limestone and Westerly granite) had a thin circumferential slot cut to a uniform depth around the central section. These were loaded in torsion about the longitudinal axis. An additional constant axial load was applied in some experiments, giving normal stresses across the expected failure plane. The loading conditions of the various samples are given in Table 1 and more details of the apparatus and mechanical technique are given in the Appendix and in Cox & Scholz (in press).

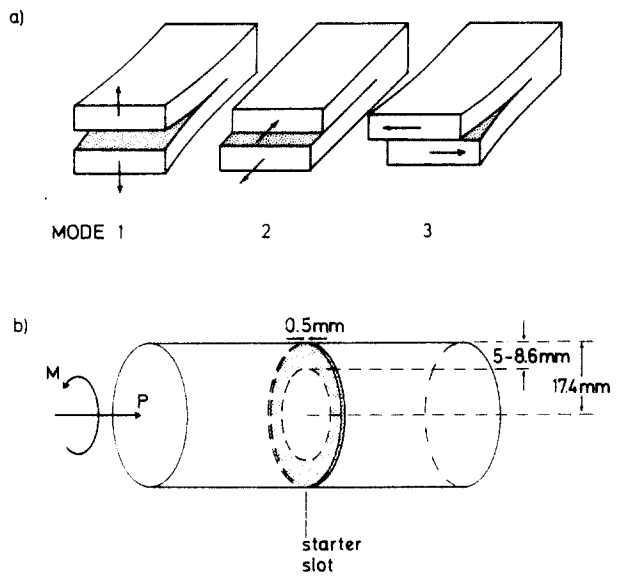

Fig. 1.(a) The three fundamental modes of fracture. (b) Experimental configuration: M—torque; P—axial force.

With purely torsional loading, this configuration has a mode 3 stress concentration, where brittle deformation initiates, all around the root of the slot. The strength of this for a sharp slit is given in standard tabulations (e.g. Tada *et al.* 1973), though the finite root radius reduces the actual value here. Since the thickness of the slot is also great enough to prevent closure of the flanks by elastic deformation under the axial loads used here, the mode 3 stress concentration is present under all the mixed loading states. The extent of failure was monitored using a compliance technique (Cox & Scholz 1988) and samples were deformed to varying total tangential (shear) displacements.

The central section of the samples (containing the notch plane and the material in the adjacent region) were removed and sections cut parallel to the specimen axis, normal to the notch plane (Fig. 2). Several parallel or oblique sectors were made from a single sample. After polishing, interior cracks piercing the surface of a section could be seen quite clearly.

Details of the section preparation and microscopy are given in the Appendix. The micrographs below are from the S.E.M. Line drawings have been copied from both S.E.M. and reflected light images.

MICROSCOPIC OBSERVATIONS

The cylindrical configuration used has a significant advantage over other configurations, in giving us a long but compact shear stress concentration, but the three-

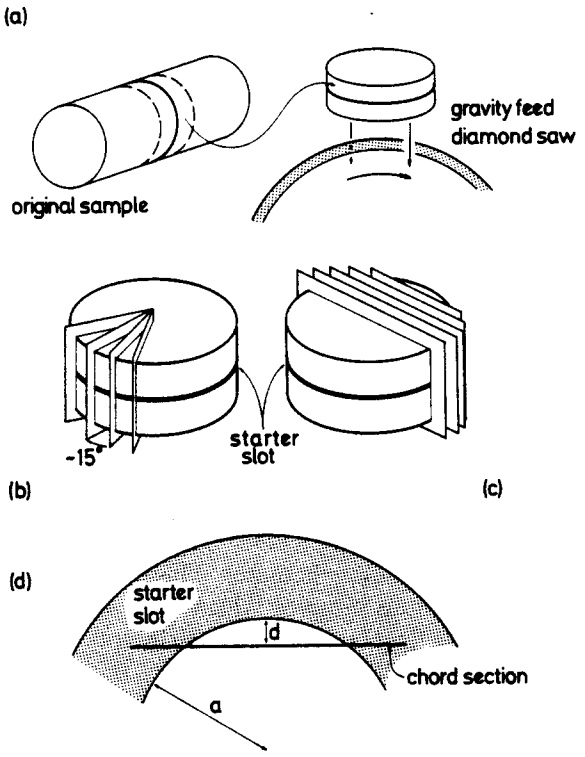

Fig. 2. Section preparation. (a) Extraction of notch section. (b) Radial section geometry. (c) Parallel section geometry. (d) Notation for location of chord sections used in examples shown here.

dimensional geometry makes it more difficult to present the results. In order to investigate the full microstructure, we had to study multiple sections from each deformed sample.

Two schemes were used to take serial sections from samples. The first was to take sections along radii of the cylinder at even spacings around an arc (Fig. 2b). Each of these spanned the transition from the starter notch to the deep interior of the sample perpendicular to the starter notch tip. The second was to take sections starting with one across the diameter and move out parallel along chords until just a short distance beneath the notch tip (Fig. 2c). This final section is mainly parallel to the notch tip.

At this scale of observation we will where possible make a distinction between *cracks* (discrete partings within or between single grains—probably showing some crystallographic control at the atomic level), *ruptures* (general brittle deformation zones clearly comprising a suite of cracks) and, at an intermediate level, *fractures* (thin brittle partings at the lower magnifications, but which may still comprise more than one crack when looked at more closely).

Radial series

A series of radial sections from a sample of Solnhofen limestone is shown in Fig. 3. Fractures had grown most of the way through this sample before an oblique surface (*c* in Fig. 3) caused a sharp load drop which forced the termination of the deformation experiment. Two particular fracture strands are indicated which can be correlated between adjacent sections. Strand *a* initially extends inwards past the center of the sample, while originating well behind the notch root. In the second section *a* is farther away from the notch plane and is not seen in the other sections. Strand *b* initially appears opposite *a* but in successive sections, as we move parallel to the notch root, it moves into the notch and past to the other side until it is in the same location as *a* was farther round the sample.

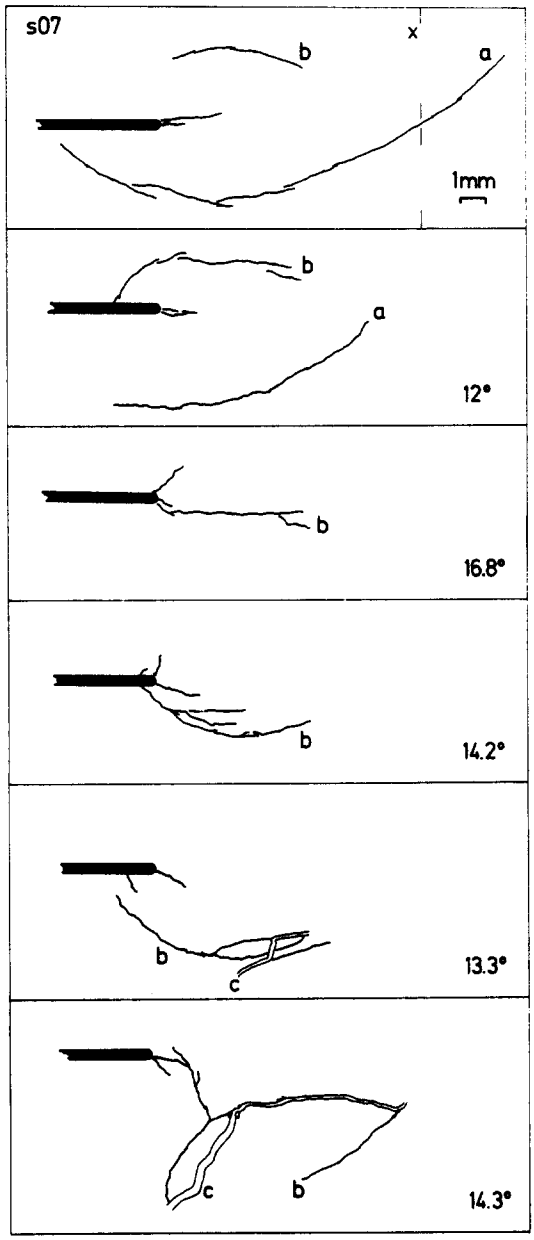

Fig. 3. Radial series of sections from Solnhofen limestone sample s07. The azimuthal spacing between adjacent sections is indicated. *a*, *b*—continuous fracture strands; *c*—catastrophic spiral fracture; *x*—axis of sample.

This sequence of the deeper fractures follows a spiraling path around the sample comparable to those observed in brittle torsional failure of a simple rod (e.g. Petrovic & Stout 1981). An idealized fracture surface may be reconstructed from these observations (Fig. 4).

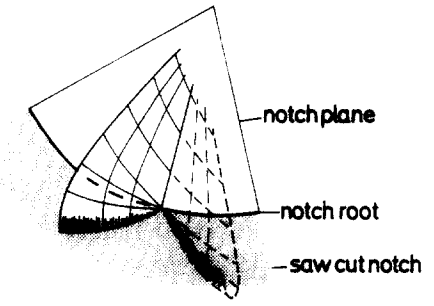

Fig. 4. Perspective view of the form of the long looping fracture surfaces shown intersecting the plane of the starter notch, as reconstructed from Fig. 3. The fracture surface is shown with cross-hatched lines, dashed where hidden beneath the plane of the starter notch, which itself is indicated by the stippling.

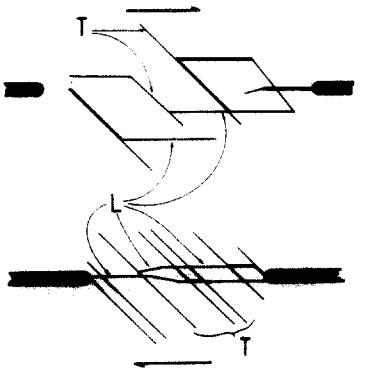

Fig. 5. Notation for the observed fracture types: *T*—oblique tensile fractures; *L*—linking fractures.

The fractures mainly follow the trajectories expected for tensile failure predicted by the initial elastic stress field. They grow into the sample in an oblique orientation and intersect at the cylinder axis (as seen by *a* in Fig. 3). Behind the notch root the traction free surfaces of the flanks of the slot cause the fractures to loop and intersect the slot in perpendicular planes.

Parallel series

In Fig. 6 we show a parallel set of sections from a sample of Westerly granite. The central sections (Fig. 6a) have pairs of fractures emerging from the notches similar to the looping fractures in the limestone (Fig. 3), though they do not intersect the slot as far behind the root. In sections successively closer to the notch root (Fig. 6b–e) we find that the parallel fractures emerge from en échelon spiral fracture arrays growing at the notch root itself. This sample has reached a relatively advanced state of rupture development and the oblique fractures have linked together to form a through-going shear zone in the region closer to the notch root (Fig. 6c–e). The linking fractures, however, do not correspond to trajectories for tensile cracks predicted by the continuum stress field.

From their relationship to the initial stress field we distinguish between the two sets of fractures genetically as well as geometrically. To simplify the discussion we use the notation indicated schematically in Fig. 5 and refer to the oblique and linking fractures as *T* and *L* fractures, respectively.

Fracture surfaces approximately parallel to the notch plane essentially envelop the *T* fracture array to form an incipient linked shear zone in Fig. 6(b) & (c). Closer to the starter stress concentration, however, the *T* fractures extend beyond the linked zone (Fig. 6d & e). In Fig. 6(e) a fairly well developed rupture cuts right through a set of closely spaced parallel *T* fractures. The net displacements on this shear zone were still very small, around 10 μm in the center of Fig. 6(e).

Development of rupture

The sequence of formation of the fracture types is suggested by an analysis of the stress state within the samples. We believe the *T* fractures formed first in response to the initial stress field. *L* fractures are formed later as the deformation increases. This interpretation is confirmed by those samples which were deformed to different total offsets under otherwise identical loading conditions (Fig. 7). The samples in Fig. 7(a) & (d) have a few widely spaced long *T* fractures only. Under increasing deformation there is a large increase in the density of short *T* fractures close to the notch plane and *L* fractures, which have local mode 2 shear displacements, break through the disrupted zone to form a complete shear rupture (Fig. 7b, c, e & f). The formation of fractures is accomplished with very little total strain in the samples. The *T* fractures are closed over most of their length and must still have considerable interaction between their walls when the *L* fractures form. The final stage of rupture development is seen at the notch root in Fig. 7(e) where the accumulated damage has led to a complete loss of cohesion of the material within the zone, so the slot has been effectively extended.

The fracture development can also be followed from the total load bearing capacity of the samples. The initiation of *L* fractures and the linking of the shear zone into alternating tensile and shear segments correlates well with the first stages of weakening past the peak torque, and increasing shear zone development leads to further reductions in the strength. This is discussed in more detail in Cox & Scholz (in press).

This model may be compared with one proposed for cyclic fatigue crack growth in steel (Ritchie *et al.* 1982) after experiments in a similar configuration. In that model, favorably oriented pre-existing flaws *ahead* of the main crack front serve as initiation sites for the shear rupture, rather than fractures growing out of the notch. This difference is due to the completely brittle nature of the materials here, compared with the ductile behaviour of metals which resists dilatation and will blunt running cracks.

We also found extreme cases of the cross-cutting *L* fractures growing directly out of the starter slot (e.g. Fig. 6e and 7a). These appeared to be the primary damage in some of the more lightly deformed samples of Solnhofen limestone. These cracks are examples of pure shear fracture growth, though the depth from the starter notch is typically limited to only about 1 mm.

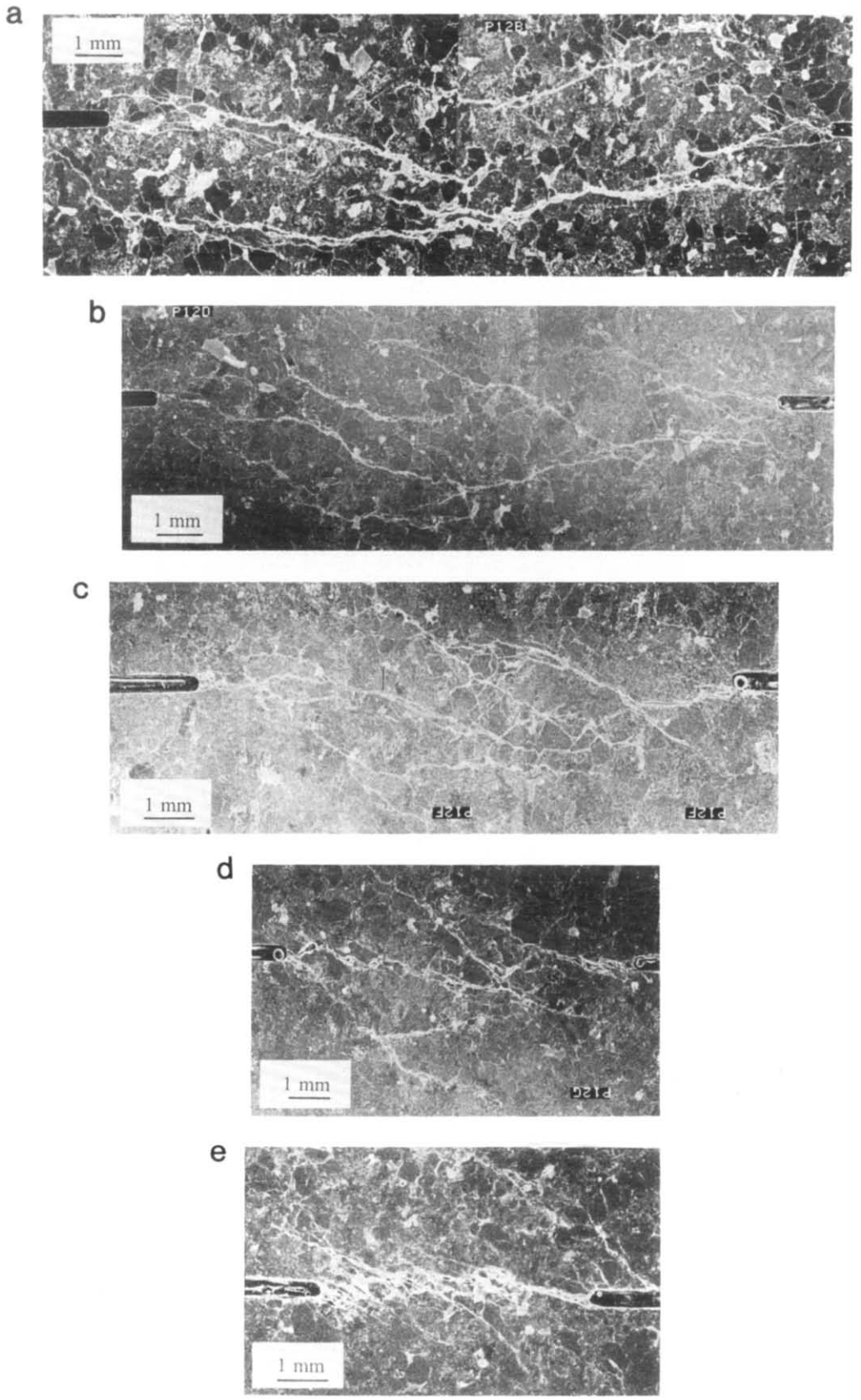

Fig. 6. Parallel series of sections from Westerly granite sample p12, parameter d is defined in Fig. 2(d). (a) d = 6.2 mm, (b) d = 4.2 mm, (c) d = 2.3 mm, (d) d = 1.4 mm, (e) d = 0.5 mm.

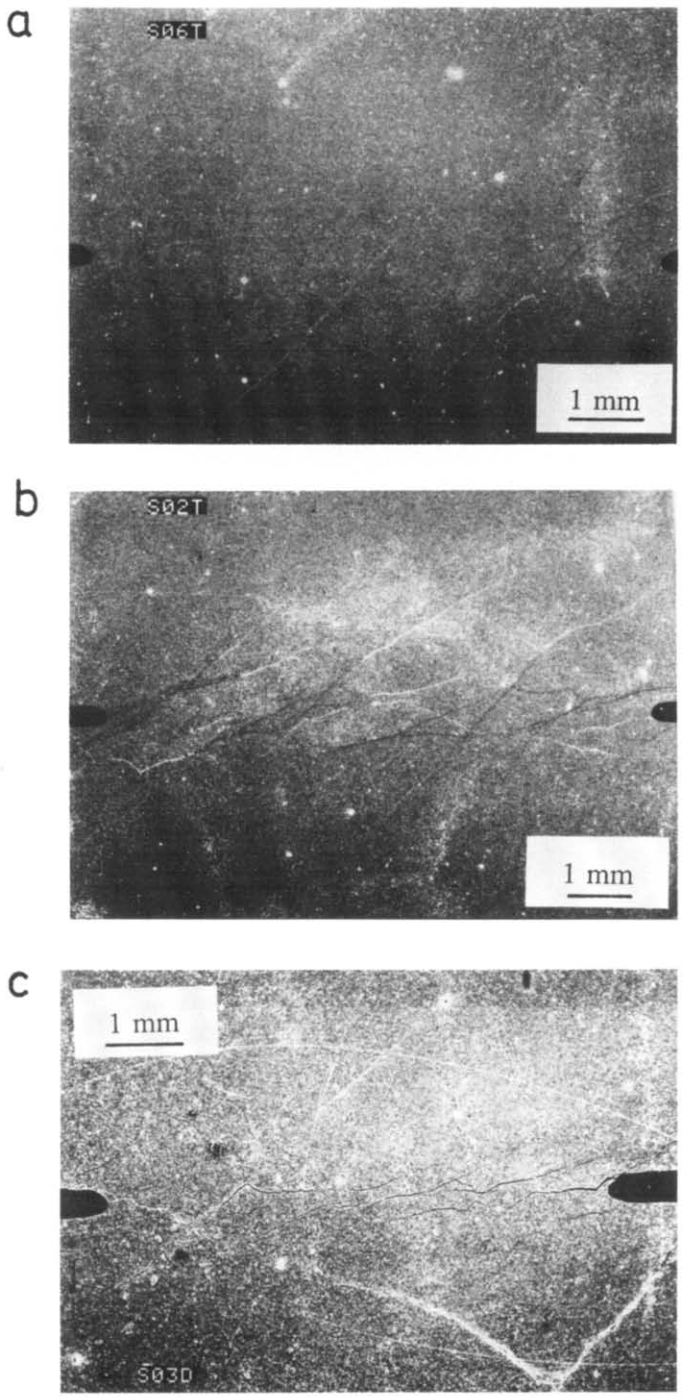

Fig. 7. The development of the shear zone. Solnhofen limestone— (a) s06, d = 0.75 mm, final offset about 350 μradians (b) s02, d = 1.2 mm, ≈600 μradians offset; (c) s03, d = 0.55 mm, ≈1350 μradians offset. *continued*

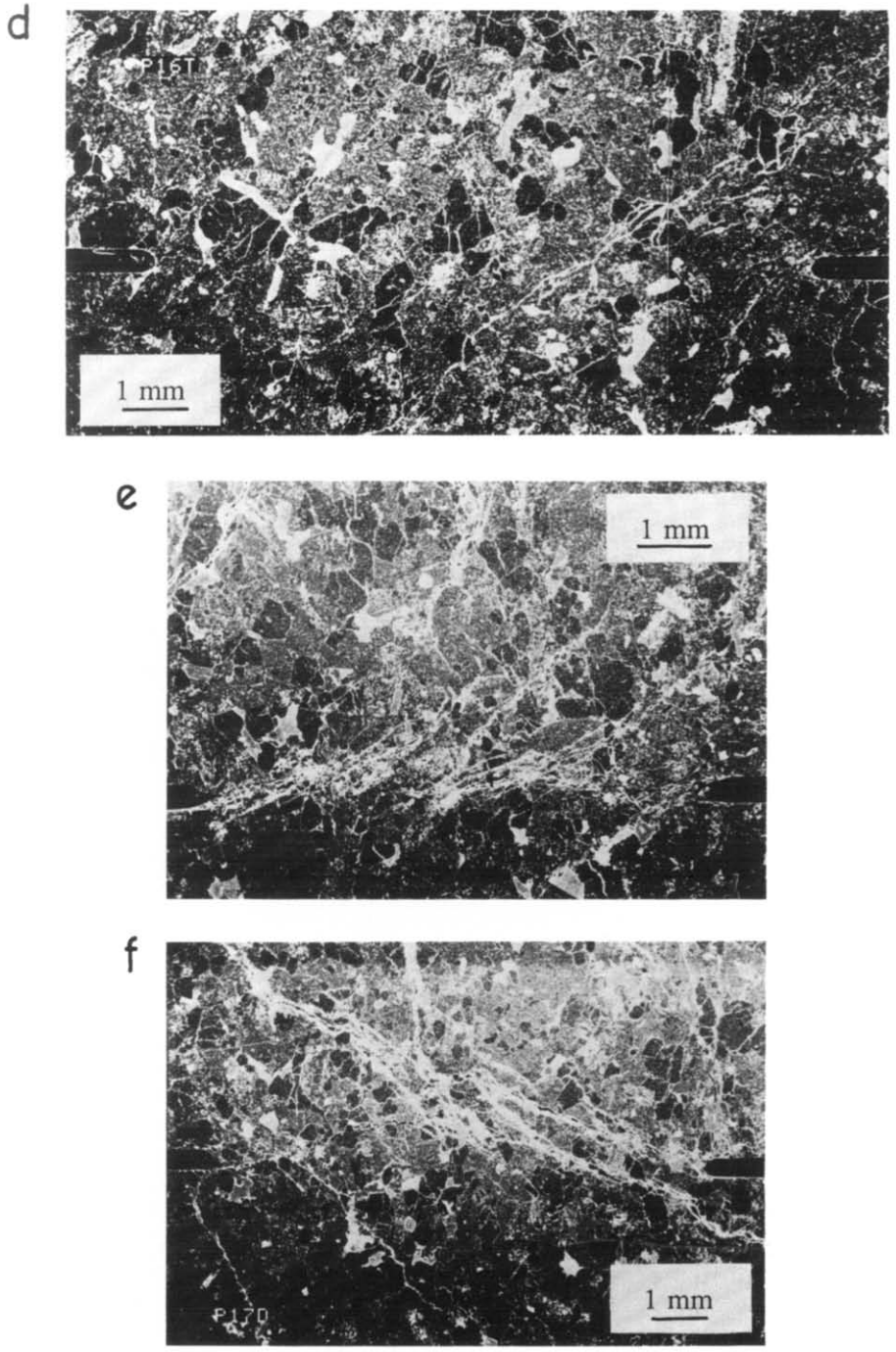

Fig. 7 *continued.* Westerly granite—(d) p16, d = 0.85 mm, final offset about 900 μradians; (e) and (f) p17, d = 0.5 mm and 1.25 mm, ≈2000 μradians offset.

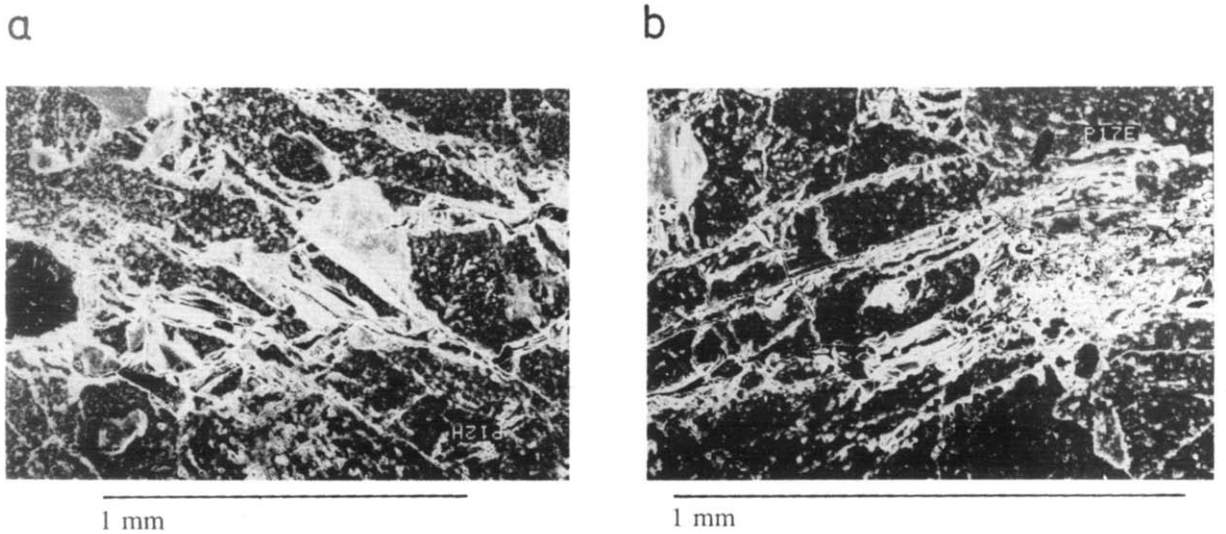

Fig. 8.(a) Detail from Fig. 6(e) showing open L fractures and rotated fragments: no axial load. (b) Detail from Fig. 7(e) showing an intense generation of T fractures intersecting a single grain: 5 kN axial load.

Orientation of T *fractures and effect of normal loads*

The predicted angle for tensile fractures in a pure shear stress field is 45°. If an axial load is added, tensile fractures will be steeper as the least compressive stress is rotated farther from the axial direction.

We found shallower angles, however, particularly in the granite, even with large applied axial stresses: adjacent to the notch and in the notch plane 20–30° is typical and this increases only farther into the sample (compare Fig. 6c with Fig. 6e and Fig. 7f with Fig. 7e).

The effect of normal loads is seen better on the longer *T* fractures. In a sequence with increasing normal loads (Fig. 9) we find the *T* fractures at progressively steeper angles to the notch plane farther away from the notch plane. At high axial loads, axial cracks mainly grow from the initial cracks that formed in the shear zone itself (e.g. in Fig. 7e). The symmetry of the torsional loads makes this effect increase towards the axis (Fig. 7f). Linked rupture zones deeper than about 2 mm beneath the notch root were unusual for samples deformed with axial loads. Complete shear ruptures across the samples, uninterrupted by a steep crack catastrophically running away, were only produced in those deformed with no axial load.

Since the *T* cracks are rarely as steep as expected in the notch plane even these have a component of true shear fracture, especially as they initially emerge from the notch root. Naylor *et al.* (1986) saw a similar pattern in their sandbox, and identified the oblique discontinuities with Reidel shears. However, those are usually considered to be a characteristic of slip in a plastic material of low dilatancy, so we will not use that terminology here for fracture in rock.

Indeed, it appears that in some cases close to the notch root, and particularly deeper into the specimens, *L* fractures have grown from *T* fractures that swung over to become parallel to the notch plane (Fig. 9b, also Fig. 6b & c). This does not account for all cases, however: close to the notch root *L* fractures usually cut right across *T* fractures (Figs. 6e and 7b & e) inhibiting further displacements on the tensile fracture strands outside of the shear zone.

Details of the shear rupture zone

In order to further illustrate the nature of the displacements and disturbance within the shear zone, we show in Fig. 8 some enlargements from the well developed shear zones already shown in Figs. 6(e) & 7(e). The *L* cracks close to the notch cut right across in an irregular fashion quite distinct from the parallel set of *T* cracks.

The effect of axial loads on the formation of the *L* cracks, and deformation within the zone can be seen clearly by comparing the samples in Fig. 8. With zero normal stress, multiple linking *L* cracks have opened up to create detached particles and grains within the zone which can be clearly seen to have rotated out of their initially interlocked positions (Fig. 8a). Although the sample deformed with a significant axial load has suffered greater permanent offset, this has been accomplished by a more intense generation of *T* cracks (Fig. 8b). The linking of the shear rupture at the higher normal stress occurs in the presence of a very high concentration of *T* cracks by the buckling of the columns between the *T* cracks, similar to that described for shear localization by Peng & Johnson (1972) and Wong (1982), rather than by a discrete generation of *L* cracks parallel to the notch plane. A similar effect, with high confining pressures producing a higher density of cracks and microcracks prior to failure, has also been described from triaxial experiments by Wawersik & Brace (1971), Kranz (1980), Wong (1982) and Wong & Biegel (1985).

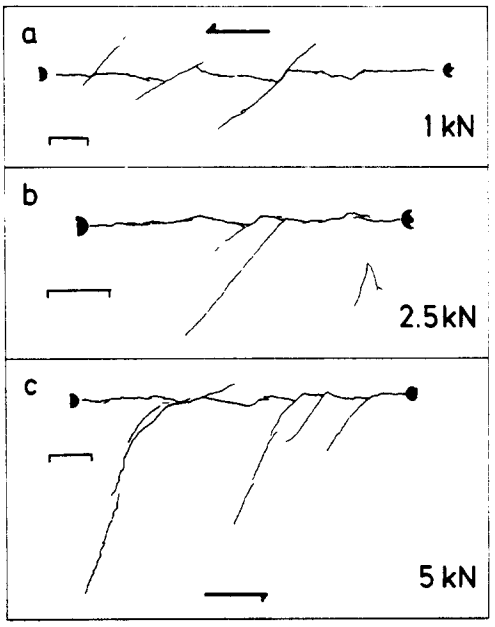

Fig. 9. The effect of normal loads on the orientation of *T* fractures and the relationship of *T* with *L* fractures in Solnhofen limestone. (a) s17, d = 1.5 mm, (b) s19, d = 0.6 mm, (c) s21, d = 0.9 mm.

A feature observed generally in the granite, but visible particularly in the higher contrast images (Fig. 7e & f) is that long *T* fractures are unaffected by grain boundaries. On the scale on which our observations were made, crystallographic control of fracture orientations along cleavage planes, as found in the feldspars by Wong (1982) does not appear to be dominant. The darker prominent grains in the micrographs are mostly quartz and, unless they intersect the boundary close to the edge of a grain, the cracks propagate right across the grains without deflection at the boundaries. In the sample shown in Fig. 8(b) parallel *T* fractures in a finely spaced array thoroughly fragment quartz grains within the shear zone and continue out undeflected by the elastic mismatch with the surrounding feldspars or discontinuities of the grain boundary. Furthermore, the effect is not simply associated with grains disturbed during the cutting of the starter slot, since the prominently fractured grains seen in Fig. 7(e) are a few grain diameters from the nearest section of the notch root behind the plane of the figure. This shows how the concentration due to the notch dominates the local stress field, over the material heterogeneity.

This contrasts with observations of microcrack dilatancy by Tapponier & Brace (1976) and crack growth by Kranz (1979a,b) who found that long microcracks in triaxially loaded samples usually involve grain boundaries and show only limited persistence across several grains. Swanson (1984) observed a greater proportion of transgranular to intergranular fractures in tensile samples fractured at relatively higher rates, but all of the samples here were fractured quasi-statically. Overall, the tendency for oblique fracture was greater if higher deformation rates were used. On a few occasions when dynamic torque loading was applied accidentally, the samples broke with just spiral fractures. When care was taken to allow complete relaxation between twist increments, shear rupture in the notch zone was successfully generated.

Effect of rock rype

We found some significantly different behaviour between the two rock types. *T* fractures in the limestone near to the notch are closer to the predicted trajectory of tensile cracks, while those in the granite seem to grow from cracks formed initially at the notch root with a shear component. The limestone samples were also more prone to uncontrolled failure by oblique or axial fractures at early stages in the deformation experiments. In samples which were deformed to approximately the same extent there is a lower total crack density in the limestone compared with the granite. Even the long *T* fractures are rarely a single strand in the granite as they are in the limestone.

This is due to the much greater initial flaw concentration in the granite, in the form of weak grain boundaries and pre-existing transgranular microcracks. Many more initiation sites for cracks are available and cracks will blunt more easily preventing them running away. The limestone, however, is well cemented and has no flaws larger than its grain size, which is much smaller than the features we are observing here; thus it behaves as a simple homogeneous elastic material. In fracture mechanics terminology, the granite is tougher (tending to absorb more energy in individual crack tips and in creating the more complex fracture strands) and the limestone is more brittle (the individual flaws, once they have formed, are much more likely to grow to a considerable length with little interaction with other cracks).

The crack density contrast is in the opposite sense to the grain size contrast. Furthermore, the overall width of the well developed shear zones, though correlating well with the grain size of the granite, rather seems to be related to the dimension of the starter slot and sample used here, since it is similar in width in the limestone whose grain size is several orders of magnitude less than the size of the saw cut.

PREDICTED STRESS FIELD

We calculate the stresses within the sample treating it as a perfectly elastic continuum. Our analysis gives the field before any damage has taken place, so should predict the formation of the initial fractures.

Analytical model

The stress field in an elastic material in the vicinity of a sharp crack may be characterized by superposition of a term with a singularity at the crack tip on to the remotely applied stress field (Lawn & Wilshaw 1975). For the general case in an infinite medium, the singular field, in a cylindrical polar system (ϱ, θ) relative to the crack tip, may be expressed as

$$\sigma_{ij} = \frac{K_n}{\sqrt{2\pi\varrho}} f_{ijn}\left(\frac{\theta}{2}\right), \tag{1}$$

where n is the mode of the applied stresses (mode 3 in this case) and f is a well defined trigonometric function. The geometrical terms describing the field may thus be separated from a term K, the stress intensity factor, which gives the strength of the singularity and includes all that is needed about the loading geometry. Expressions giving K as a function of applied stress have been compiled for many specific geometries by a number of authors (Paris & Sih 1965, Tada *et al.* 1973, Rooke & Cartwright 1976).

The symmetry of our configuration makes the shear stresses zero at the axis, overriding the prediction of equation (1) at this distance from the notch. Likewise, the free surface of the rod cannot support the tractions implied by equation (1). For the case of a long rod with a torque M applied at the ends, which has a deep circumferential notch leaving an intact ligament of radius a, Harris (1967) derived an expression for K_3 from stress concentration factors given by Neuber (1958)

$$K_3 = \frac{3M}{4\sqrt{\pi a^5}} \tag{2}$$

and Neuber also gave a solution for the shear stress component τ_θ at radius r in the notch plane

$$\tau_\theta = \frac{3M}{4\pi a^3}\frac{r}{a}\left(1 - \frac{r^2}{a^2}\right)^{-1/2} \tag{3}$$

which may be expressed in terms of the stress intensity factor, equation (2), as

$$\tau_\theta = \frac{K_3}{\sqrt{\pi a}}\frac{r}{a}\left(1 - \frac{r^2}{a^2}\right)^{-1/2}. \tag{4}$$

Comparing this with the solution for an infinite medium given by equation (1), we find that the stresses within the intact part are modified by a factor

$$\sqrt{2}\,\frac{r}{a}\left(1 + \frac{r}{a}\right)^{-1/2} \tag{5}$$

giving zero at the axis. We may assume that this factor will also apply to the other stress components, giving us the full elastic solution for that part of the sample $r < a$.

In Fig. 10(a) we show the stress field on a section across a diameter of the sample, calculated using equation (1) modified by equation (5) for the case of a sharp

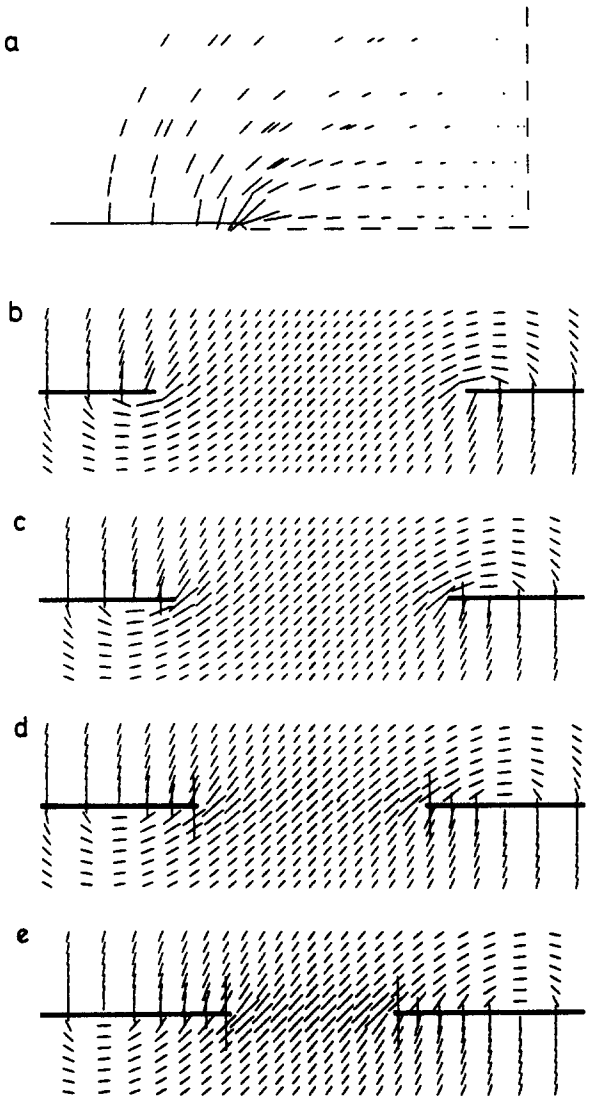

Fig. 10. Stress field in the sample from the analytical solution for the initial configuration. The ticks plotted are vectors aligned parallel to the intersection of the plane of this projection with the plane normal to the least compressive (or greatest tensile) stress. The lengths of the vectors are proportional to the differential stress (greatest–least). The ticks are thus the expected orientation and 'strength' of any tensile cracks formed in the interior of the sample due to the initial stress field (before any damage had occurred). (a) Radial plane. (b)–(e) Chord sections with d/a = 0.28, 0.21, 0.14 and 0.07.

slot under pure torque loading. This projection plane was chosen to give an overview of the stress field throughout a specimen and was usually the first section studied from the samples. Figure 10(b)–(e) shows sections across chords of the notch plane parallel with the axis of the cylinder. Figure 10(e) is almost completely parallel to the direction of shear loading at the root of the notch.

We see from Fig. 10 that the T cracks in the samples are the brittle response to the tensile stresses in the field generated by the torque loading. With no axial load, purely tensile cracks will make an angle of 45° with the notch plane, though we expect the fractures to become 'opportunistic' as the magnitude of the stress field diminishes towards the axis and depends more on the location of the earlier formed fractures for their locations in the center of the sample. Figure 10(a) also shows how the looping form of the cracks intersecting the notch behind its root is predicted by the stress analysis. The L cracks seen in the interior of the samples, particularly closer to the notch, are not predicted from the initial elastic stress field.

Wong (1982) calculated the deflection of the optimum tensile crack orientation from the directions predicted in a homogeneous stress field due to the elastic anisotropy of the component minerals in Westerly granite and found that variations of up to 12° could be explained this way in the feldspars, though only 5° in quartz. This is clearly insufficient to account for the deviations of 20–25° observed here, which were also in long fractures transacting several grains, so cannot be explained by models of the elasticity of single grains.

From the symmetry of the configuration, the normal stress distribution in the notch plane is that of a rigid circular indenter into a half space under remote normal force P,

$$\sigma_n = \frac{P}{2\pi a^2}\left(1 - \frac{r^2}{a^2}\right)^{-1/2} \tag{6}$$

(Boussinesq 1885). There is a singularity in the normal stress, equation (6), as well as the shear stress, equation (3), at the notch root. The normal stress concentration is not as strong, but the normal stress has a finite value across the notch plane, while the shear stress decreases to zero at the axis. A significant disadvantage of this experimental configuration, therefore, is that towards the axis of the cylinder, the overall field becomes dominated by the uniaxial field. For the samples deformed with an axial load we do not expect rupture to grow in a shear plane right across the sample, so only the observations towards the outside of the rupture zone are relevant to the problem being addressed here.

Numerical model

A numerical method was used to model the overall stress field for the more detailed case here (with the finite boundaries, a less sharp notch and a superimposed compressive axial load). We devised a three-dimensional finite-element mesh with 500 elements and 563 nodes (Fig. 11), and studied the static elastic response using the ADINA (1981) package. The eigenvectors for stress at the Gauss-integration points were computed using the method of successive approximation (Nye 1985).

The mesh was constructed to give finer detail close to the notch tip and coarser away from it. However, some deflection of the stresses appears to have been introduced where degenerate element geometries had to be used, suggesting that a more uniform finer mesh may improve results.

We ran experiments to simulate the suite of loading conditions used in the laboratory. These included two end members with pure torque and pure axial load, and combinations with the torque held fixed and a varying axial load. Figure 12 shows the stress field projected on to a radial plane for three cases.

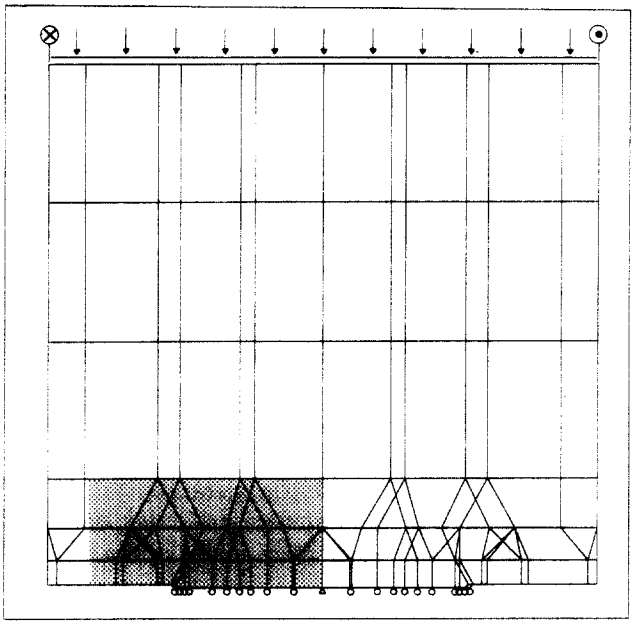

Fig. 11. Cross-section through three-dimensional finite-element model. The projection shows the edges of the elements covering a radial plane. The shaded area is the zone for which the results are plotted in Fig. 12. Loading at top—tangential point loads at the rim and uniform pressure parallel to the axis; constraints at bottom—centre node fixed in all directions, nodes in the intact notch plane free in radial direction only.

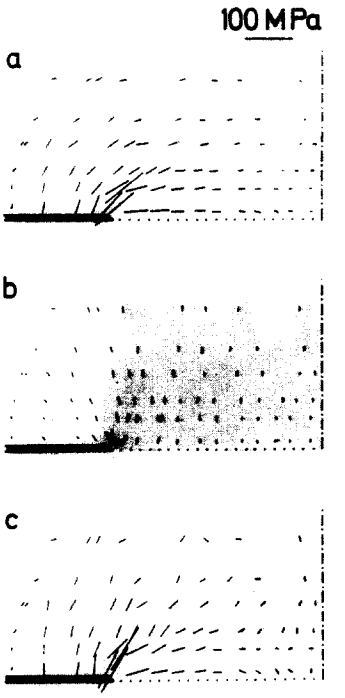

Fig. 12. Predicted tensile fractures on a radial plane from the finite-element model. Shaded zone is where all the stresses are compressive. (a) 50 Nm torque, zero axial load, (b) 5 kN axial load, zero torque, (c) 50 Nm torque and 5 kN axial load.

We may compare Fig. 12(a) (the numerical case for pure torque) with Fig. 10(a) (the analytical case plotted for the same points on the same radial plane) to determine the success of the numerical model. Figure 13 shows a radial stress profile determined using the two methods. In the core of the sample, where our observations were made, the two methods agree very well, while the analytical solution overestimates the stress magnitude towards the outer surface of the sample as expected.

The effect of the axial loads in the range used is mostly outside the notch zone. In the mixed loading case (Fig. 12c) the two rows of stress vectors closest to the notch plane are in nearly the same orientation as for pure torsion (Fig. 12a). This emphasizes the dominant effect of the strong stress concentration on the stress field. Only farther from the notch zone do the axial stresses become important and tensile cracking at these distances from the plane is expected to become dominantly axially oriented. In Fig. 12 we also show the areas where all normal components of the stress tensor are compressive. Applying axial loads expands this zone in the core of the sample, while the torsional load re-establishes tensile stress components in the region adjacent to the stress concentration.

Figure 14 shows a sequence of sections across the diameters of samples deformed at increasing axial loads. The zone of fracturing growing from the notch gets wider as the axial load is increased and axially oriented cracks are seen at first just towards the centers of the samples, as expected from the normal stress distribution. At the higher loads axial cracks dominate right across the zone. Comparing the distribution of internal cracks seen here to the stress field (Fig. 12), we find that fracture is mainly confined to the regions where one of the principal stresses is tensile.

In a case of polyaxial compression, however, we would expect the additional stresses normal to the axial direction to stabilize crack growth in that direction (Nemat-Nasser & Horii 1982). Stereological studies have also shown how increasing the confining pressure in samples deformed under triaxial loading leads to a significant reduction in anisotropy of microcrack development (Wong 1982, Wong & Biegel 1985). This suggests that outside of the zone, where tensile stresses dominate due to the stress concentration, fracture may not continue to propagate just in this axial direction. Thus the

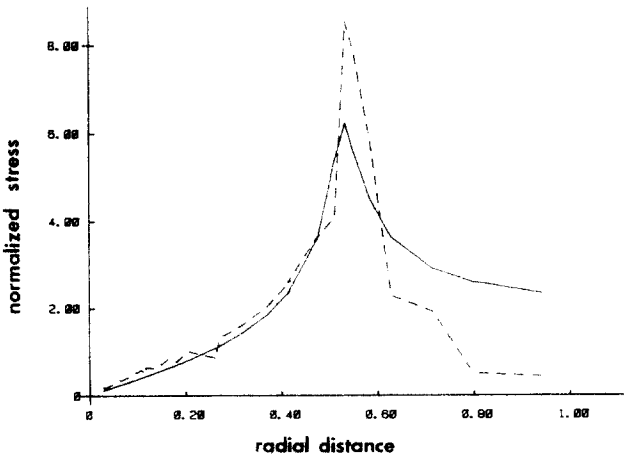

Fig. 13. Normalized shear stress magnitudes along the row of points closest to the notch plane from Figs. 10(a) and 12(a). (——) analytic solution; (– –) numerical solution. The radial position is normalized to the cylinder radius: the notch tip is at 0.537.

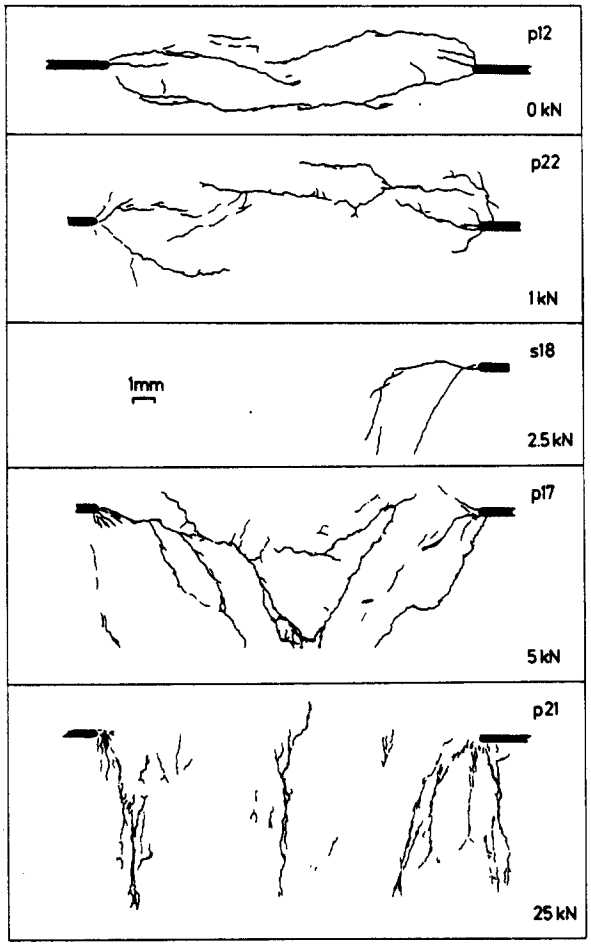

Fig. 14. Effect of axial loads on the fracture patterns in the interior of samples—these sections are across the diameter of the samples.

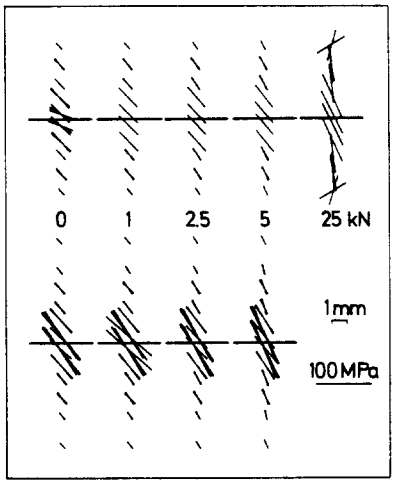

Fig. 15. Effect of axial loads on the predicted tensile fractures on chord planes close to the notch root. Results shown from the finite-element model: horizontal dashed line = notch root, diagonal lines = stress vectors. (In some cases several stress vectors are superimposed making the vectors look heavier.) Top—$d/a = \approx 0.11$. Bottom—$d/a = \approx 0.35$.

problem of the widening of the damage zone seen so dramatically at the higher axial loads may be mitigated under natural conditions due to the more uniform compressive stress field and the absence of zeros in the shear stress field, compared to the torsional geometry.

In Fig. 15 we show projections of the stress field on chord planes a small distance beneath the notch root, as computed using the model for a variety of axial loads. This projection corresponds to the central fibers of the chord sections (Fig. 10b–e). Even for quite large normal loads the orientation of the tensile stresses close to the stress concentration are not changed very much. Again, we see the importance of the stress gradient imposed by the slot behind the plane of the figure, and thus, the significance of the full three-dimensional geometry we are examining here.

A model with softened elements in the zone where fracture is expected to initiate was also examined. We modified the elastic constants of the elements immediately beneath the starter notch to reduce the modulus of rigidity by varying amounts. This simply had the effect of reducing the intensity of the stress concentration, thus transferring some of the load to the regions of the sample outside of the vicinity of the starter notch. The more serious effect of weakening in the central zone, however, is in concentrating the strain. Of course, if the central zone elements are made weaker by an inelastic process, then a limit on the stress that can be supported will localize all subsequent deformation here. These effects have not been incorporated into our finite-element model, since heterogeneous and time dependent material properties have to be used.

Multiple crack models

In order to investigate the stress field within the disrupted zone, we need to introduce the T cracks into the elastic model. We have not attempted that explicitly here, so we will review some related studies that may indicate likely results.

Peng & Johnson (1972) presented a treatment of shear localization by buckling of an array of columns between microcracks formed parallel to the principal compressive stress. A limiting fiber stress on the surface of the beams was used for the failure criterion, producing a set of failure envelopes which described their macroscopic observations in triaxial loading. However, though the model was based on micromechanical considerations, the statistical approach precluded prediction of specific local fracture geometries in the rupture zone.

We initially consider the two-dimensional field around two staggered parallel cracks. Kranz (1979b) simply superposed the stress fields computed for isolated cracks (his fig. 3), and found a slight tensile stress concentration between the tips of non-overlapping tensile cracks, which may form the nucleus of the L fractures. In a review of models of a single crack inclined to the principal stresses, however, Sobolev & Shamina (1975) showed that cohesion across the crack can have a significant effect on the distribution of the stress field, although model experiments described by Shamina *et al.* (1975) still produced tensile cracks from the tip of an inclined slot whose walls were in contact.

Segall & Pollard (1980) used a numerical method to

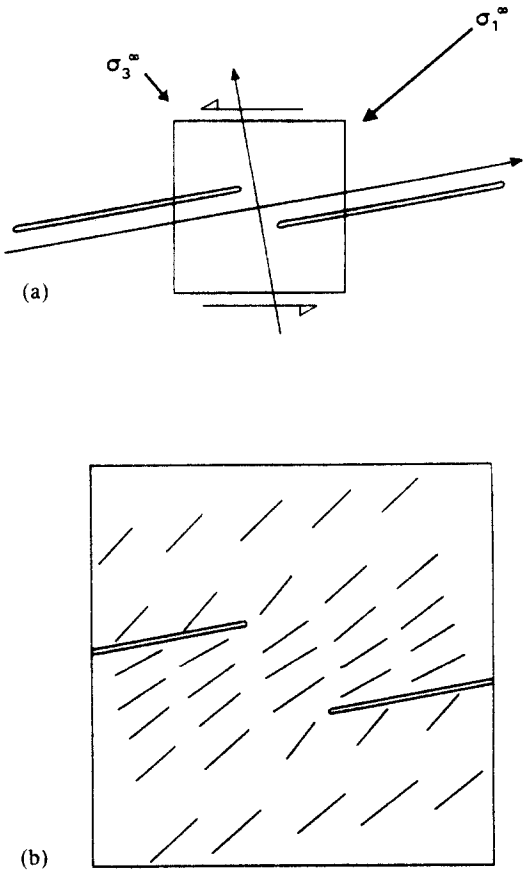

Fig. 16. (a) Geometry for calculating the two-dimensional stress field modified by two non-coplanar fractures. (b) The predicted next generation of tensile fractures (from Gamond 1983. Reprinted with permission, Copyright 1983, Pergamon Press Ltd. and after Segall & Pollard 1980).

analyze the field around a specific array of cracks, also including tractions on the walls of their initial cracks. The geometry in Fig. 16(a) sets up a problem similar to our arrays of T fractures: initial en échelon cracks at a shallow angle to the greatest principal stress, σ_1^∞. The expected orientation of the next generation of tensile cracks shown in the solution in Fig. 16(b) indicates that, at least when the overlap between T fractures is small, new *tensile* cracks do not tend to link the T fractures. Thus, the L cracks we see in our samples appear to be true shear cracks.

The effects of the whole suite of cracks in the true three-dimensional sample geometry seen in our experiments will be more complicated than such simple continuum models. In particular these do not allow for the strong stress gradient caused by the slot outside of the plane of the two-dimensional crack arrays described. A calculation of the local stress field at each stage for this geometry, however, requires an incremental approach to the elastic modeling beyond the scope of the present study.

A MODEL FOR SHEAR FRACTURE?

These experiments have demonstrated some important features of shear rupture development using a technique which is complementary to previous studies in three significant ways: (1) we have grown shear rupture zones in a controlled way and predictable location by using a stress concentrator–fracture mechanics type configuration; (2) by using a mode 3 stress concentration we generated a pattern of deformation which requires a consideration of the full three-dimensional nature of the stress field and crack arrays; (3) our studies of the crack interaction are at a scale intermediate to previous investigations, either of microcrack development on a grain size scale or of fault interactions in the field.

The first two of these features may be related. Previous experimental studies of crack growth from a well defined shear stress concentration (Brace & Bombolakis 1963, Lajtai 1971, Shamina *et al.* 1975, Ingraffea 1981) used essentially two-dimensional configurations to study mode 2 (in-plane shear) loading. Rupture extension as a single crack which follows the compressive stress trajectory is compatible with the displacement field around a mode 2 concentrator. From a mode 3 stress concentrator, however, a suite of initial cracks formed en échelon at the notch root accommodates the shear displacements. Subsequent development may be dominated by interactions between these flaws, to produce a shear rupture (Brace & Bombolakis 1963, Wong 1982) with a single one of these oblique cracks unable to run away to take up the whole deformation. The complex stress field around such an extended concentrator may be necessary for true shear rupture extension.

Since a single tensile crack will develop only from a pure mode 2 stress concentration, multiple oblique cracks are generally expected to form around a shear crack. Taking a discontinuity initially loaded in shear as the primary feature, the growth of tensile secondary cracks from its tip has been demonstrated in studies in the field (e.g. Granier 1985) and the laboratory. These studies, therefore, have considered the first stage of rupture growth only. Here we have generated the next stages of shear rupture development—the linking of the initially formed tensile cracks by shear cracks and internal deformation of the rupture zone with increasing shear displacements.

We tentatively propose a multi-stage model for brittle shear rupture growth. An initial planar shear stress concentrator causes the formation of an array of 'tensile' cracks close to the tip; with subsequent shear deformation, shear cracks form which link and intersect the tensile cracks to enclose a zone of debris (microbreccia) whose thickness is of the order of the width of the initial stress concentration. Finally, when internal deformation has caused sufficient cohesion loss in the brecciated zone, the extended rupture zone is the source for a subsequent generation of tensile crack formation.

Comparing this to two-dimensional models of brittle rupture localization in triaxial experiments by Peng & Johnson (1972) and Wong & Biegel (1985), the additional feature here is a concentration of the shear stress by an initial elastically contrasting inclusion outside the plane considered in those studies.

A crucial element of the geometry is the width of the

developing rupture zone. For the formation of long discrete faults a mechanism is required to prevent any single tensile crack running away, or the fractured region growing continually in width until general, rather than localized, shear deformation is taking place ('damping' of Granier 1985). There is some tendency for cracking to spread away from the notch plane, particularly at higher axial loads. However, in those samples which were deformed sufficiently to cause damage right across the diameter, the fracture arrays are still confined within a small zone close to the notch plane and generally strain will be concentrated into the softened zone. Once formed, the cross-cutting shear cracks suppress subsequent extension and deformation on those parts of the *T* fractures outside of the zone. Furthermore, in an overall compressive stress field the stresses normal to the *T* fractures outside of the shear zone will act to stabilize the growth of the tensile cracks there.

We may also interpret the deformation extending right across samples as a model of how coplanar cracks link up under shear loading, or as the rupture of an 'asperity' on an earthquake fault (Das 1986).

Regarding the scales, the cracks we studied here are not, on the whole, on cleavage planes, such as most of those shown by Tapponnier & Brace (1976), Kranz (1979a) and Wong (1982). Those are subject to strong crystallographic control and may indeed be consistent with a simple energy-balance understanding of fracture mechanics prediction. The fact that transgranular *T* fractures follow the stress trajectories as well as they do in the granite requires that the fractures be compound at the crystallographic level, at least as linked cleavage cracks. In many of the granite sections fractures are made up of several irregular strands; in the fine-grained limestone we could not distinguish between transgranular and intergranular cracks, but fracture strands typically encompass a few grain widths. However, the zone contained within the complete shear zone across the sample is narrow (less than 5 mm wide in Fig. 6 for example), so the rupture zones produced are still essentially sharp and planar on the scale that field observations are made. Large-scale shear fractures may yet encompass several of these small features while developing into well developed fault zones.

DISCUSSION AND IMPLICATIONS

Our model of damage zone control of fracture development is similar to Griffith's (1920) hypothesis of the critical flaw which leads to tensile failure. We find here, however, that multiple flaws are necessary for shear fracture development.

An initial damage zone, or *process zone*, has been frequently hypothesized in fracture mechanics to explain the greater energy dissipation found in the fracture of polycrystalline materials than expected from the fracture energy of the constituent phases. Recently an alternative model has been proposed which dispenses with a distributed damage zone in the formation of tensile ruptures in brittle materials (Swanson 1987). In the generation of shear ruptures, however, the *process zone* appears to be a crucial component (Brace & Bombolakis 1963, Wong & Biegel 1985).

An array of cracks may form in several ways. In conventional triaxially loaded cylinders, axially oriented microcracks form throughout the sample, with deformation localizing onto an arbitrarily oriented single plane at a relatively late stage when the overall crack concentration is high throughout. Alternatively, as demonstrated here, an existing plane of stress concentration will cause localized damage at lower applied loads, which acts as the locus for subsequent rupture development. The origin of this initial discontinuity may be from a number of sources, certainly including tensile fractures (joints) as suggested by Segall & Pollard (1983).

The development of an array of en échelon cracks from the tip of a parent crack in the field has been described by Pollard *et al.* (1982) and Etchecopar *et al.* (1986). The mechanical model proposed by Pollard *et al.* includes a tensile stress on the parent crack to explain dilatant echelon cracks. In the general case oblique 'tensile' cracks will form even without a remote applied tensile stress, although not opening significantly. The damage leading to rupture extension will form preferentially where the stress has at least one locally tensile component; although a case of tensile fracture extension under conditions of overall compressive stress has recently been described by Scholz *et al.* (1986). We thus have a mechanism for elevated pore pressure to affect the development of shear rupture, comparable to the dominant influence it has on joint formation or tensile rupture (Engelder 1985).

If shear rupture formation is always preceded by oblique tensile fracturing, then we might expect to see some evidence of this as a damage zone around faults. In a study of a fault in California, Chester & Logan (1986) noted a well defined disrupted area adjacent to the zone where slip is concentrated, with subsidiary faults forming a "diffuse, but generally conjugate, set". We suggest that they are broadly aligned in the direction of our *T* fractures and represent evidence of the way their fault formed. Where high fluid pressures are involved in hydrothermal systems this could also involve the deposition of vein material in dilatational fractures. This provides a rationale for the common field practice, when mapping in low-grade terranes with small exposure, of finding nearby faults by the presence of veining. Scholz (1987) has also found that the rate of formation of gouge in natural faults is much greater than that found in the wear of artifically prepared surfaces. This would be expected if the wall-rock around the initially formed shear rupture is as disrupted as we suggest here.

More orderly arrays of dilatational cracks associated with semi-brittle shear zones have often been observed in the field. Knipe & White (1979) deduced three stages in the evolution of some shear zones in a low grade arenite, finding that an en échelon zone of oblique fracturing was the first step in the localization of deformation even in this case, where subsequent strain was mostly by plastic and diffusional processes.

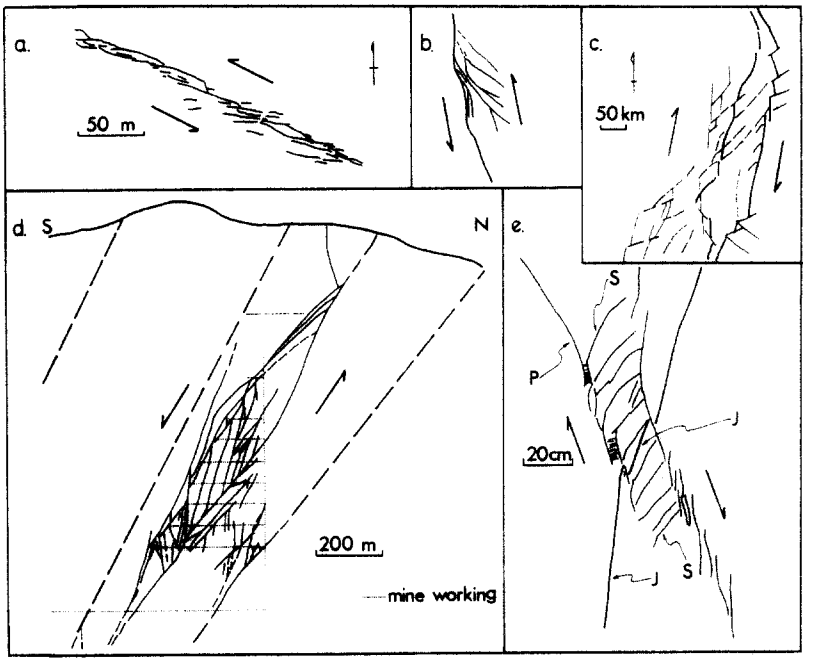

Fig. 17. Examples of complex fault zones. (a) Dasht-e-Bayaz, Iran, (b) Ales, France, and (c) Taranaki graben, New Zealand—(a)–(c) all map views adapted from Naylor *et al.* (1986). (d) Cross-section through a fault array in the Coeur d'Alene mine, Idaho, compiled from observations in an extensive series of mine galleries (shown as thin dotted lines, after Wallace & Morris 1986). (e) Fresh fracture in a deep mine, Republic of South Africa (after McGarr *et al.* 1979). J—pre-existing joint, P—primary and S—secondary fractures as described by McGarr *et al.* (1979).

Quite generally, when a complete investigation of the three-dimensional geometry of large faults is made, they are found to be composed of multiple anastomosing strands (Fig. 17). In the map views in Fig. 17(a)–(c) the oblique and splay faults all have the correct orientation to have initiated as *T* fractures. Sharp (1979) suggested that such complexity in fault traces may be mainly a surface phenomenon with the geometry simplifying at depth; however, in a steeply dipping normal fault mapped underground (Fig. 17d) we find that a fault that is mapped as a single trace at the surface is comprised of an extensive zone of fracturing at depth. In a unique study of a freshly formed shear fracture zone in a mine, McGarr *et al.* (1979) found a fracture array (Fig. 17e) whose geometry bears remarkable similarity to some of our sections. On the basis of our model, however, we would relabel their primary fractures (*P* in Fig. 17e) as tertiary or *L* fractures, with the primary (stress concentrating) fracture being out of the plane of the sections that they studied. The existence of the mine excavation would introduce local tensile stresses in this case. It is also interesting to note that a pre-existing joint (*J* in Fig. 17e), which crosses the shear zone, is in the same orientation as the secondary (*T*) fractures within the zone. Thus, it may have formed under the same stress field before the deformation was concentrated into the zone observed by the *L* fractures, which cut across it in a fashion similar to that seen in our sections.

We must have some caution in our comparisons however, as McGarr *et al.*'s (1979) structure formed in a seismic event, hence much of the fracturing may have been dynamic. These observations have been made at scales much larger than our microscopic investigation, so we only draw attention to the gross similarities between the geometries in Fig. 17 and the micrographs.

CONCLUSIONS

From a careful study of the geometry of fracture formation induced by a large shear stress concentration in rock, we now think that under certain circumstances, a shear fracture zone may extend in length and in its own plane. A dominantly mode 3 stress concentration has a greater likelihood of in-plane extension than mode 2 due to its initially more complex damage zone and three-dimensional constraints. Subsequent development is in the presence of a stress field modified by the first formed tensile cracks. A complete theory of shear rupture growth is not possible at this time, but we believe that we have suggested components that need to be considered and some of the ways we can identify these in the Earth.

Acknowledgements—This work was supported by NSF under contracts EAR81-20318 and EAR84-08348. We would like to thank Dee Breger for assistance with the S.E.M., and Shamita Das and Barry Raleigh for reviews. Lamont-Doherty Geological Observatory contribution No. **4264**.

REFERENCES

ADINA 1981. Automatic dynamic incremental non-linear analysis (software). Adina Engng Inc., Watertown, Massachusetts.

Anderson, C. M. 1951 *The Dynamics of Faulting*. Oliver and Boyd, Edinburgh.

Boussinesq, M. J. 1885. *Application des Potentiels* . . . . Gauthier-Villars, Paris.

Brace, W. F., 1960. An extension of the Griffith theory of fracture to rocks. *J. geophys. Res.* **65**, 3477–3480.

Brace, W. F. & Bombolakis, E. G. 1963. A note on brittle crack growth in compression. *J. geophys. Res.* **68**, 3709–3713.
Chester, F. M. & Logan, J. M. 1986. Implications for mechanical properties of brittle faults from observations of the Punchbowl fault zone, California. *Pure Appl. Geophys.* **124**, 79–106.
Cox, S. J. D. & Scholz, C. H. In press. Rupture initiation in shear fracture of rocks. *J. geophys. Res.*
Das, S. 1986. Comparison of the radiated fields generated by the fracture of a circular crack and a circular asperity. *Geophys. J. R. astr. Soc.* **85**, 601–615.
Engelder, T. 1985. Loading paths to joint propagation during a tectonic cycle: an example from the Appalachian Plateau, U.S.A. *J. Struct. Geol.* **7**, 459–476.
Etchecopar, A., Granier, T. & Larroque, J.-M. 1986. Origin des fentes en echelon: propogation des failles. *C.r. Acad. Séanc. Sci., Paris* **302**(II), 479–484.
Gamond, J. F. 1983. Displacement features associated with fault zones: a comparison between observed examples and experimental models. *J. Struct. Geol.* **5**, 33–45.
Gamond, J. F. & Giraud, A. 1982. Identification des zones de faille a l'aide des associations de fractures de second ordre. *Bull. Soc. géol. Fr., 7 ser.* **24**, 755–762.
Granier, T. 1985. Origin, damping, and pattern of development of faults in granite. *Tectonics* **4**, 721–737.
Griffith, A. A. 1920. The phenomena of rupture and flow in solids. *Phil. Trans. R. Soc. Lond.* **A221**, 163–198.
Harris, D. O. 1967. Stress intensity factors for hollow, circumferentially notched round bars. *J. Basic Engng* **89**, 49–54.
Holzhausen, G. R. 1978. On the propagation of fractures inclined to the direction of uniaxial compressive stress in a rock-like material, Westerly granite and plexiglass, *Norwegian Geotechnical Inst, Internal report* 54102–1.
Horii, H. & Nemat-Nasser, S. 1985. Compression-induced microcrack growth in brittle solids: axial splitting and shear failure. *J. geophys. Res.* **90**, 3105–3125.
Ingraffea, A. R. 1981. Mixed-mode fracture initiation in Indiana limestone and Westerly granite. *Proc. 22nd U.S. Symp. Rock Mech.*, 186–191.
Knipe, R. J. & White, S. H. 1979. Deformation in low grade shear zones in the Old Red Sandstone, S.W. Wales. *J. Struct. Geol.* **1**, 53–66.
Kranz, R. L. 1979a. Crack growth and development during creep of Barre Granite. *Int. J. Rock Mech. Min. Sci. Geomech. Abs.* **16**, 23–35.
Kranz, R. L. 1979b. Crack–crack and crack–pore interactions in stressed granite. *Int. J. Rock Mech. Min. Sci. Geomech. Abs.* **16**, 37–47.
Kranz, R. L. 1980. The effects of confining pressure and stress difference on static fatigue in granite. *J. geophys. Res.* **85**, 1854–1866.
Lajtai, E. Z. 1971. Experimental evaluation of the Griffith theory of brittle failure. *Tectonophysics* **11**, 129–156.
Laqueche, H., Rousseau, A. & Valentin, G. 1986. Crack propagation under mode I and II loading in slate schist. *Int. J. Rock Mech. Min. Sci. Geomech. Abs.* **23**, 347–354.
Lawn, B. R. & Wilshaw, T. R. 1975. *Fracture of Brittle Solids.* Cambridge University Press, Cambridge.
McGarr, A., Pollard, D. D., Gay, N. C. & Ortlepp, W. D. 1979. Observations and analysis of structures in exhumed mine-induced faults. In: *Proc. Conf. VIII—Analysis of actual fault-zones in bed rock.* USGS Open File Report No. 79–1239, 101–120.
Naylor, M. A., Mandl, G. & Sijpesteijn, C. H. K. 1986. Fault geometries in basement-induced wrench faulting under different initial stress states. *J. Struct. Geol.* **8**, 737–752.
Nemat-Nasser, S. & Horii, H. 1982. Compression induced non-planar crack extension with application to splitting, exfoliation, and rock burst. *J. geophys. Res.* **87**, 6805–6822.
Neuber, H. 1958. *Theory of Notch Stresses.* AEC-tr-4547, Office of Technical Services, Dept of Commerce, Washington, D.C.
Nye, J. F. 1985. *Physical Properties of Crystals*, 2nd edn. Oxford University Press, Oxford.
Ohnaka, M. 1973. The quantitative effect of hydrostatic confining pressure on the compressive strength of crystalline rocks. *J. Phys. Earth* **21**, 125–140.
Paris, P. C. & Sih, G. C. 1965. Stress analysis of cracks. *Am. Soc. Mat. Spec. Tech. Publ* **381**, 30–81.
Petrovic, J. J. & Stout, M. G. 1981. Fracture of Al_2O_3 in combined tension/torsion: 1. Experiments. *J. Am. Ceramic Soc.* **64**, 656–660.
Peng, S. S. & Johnson, A. M. 1972. Crack growth and faulting in cylindrical specimens of Chelmsford granite. *Int. J. Rock Mech. Min. Sci. Geomech. Abs.* **9**, 37–86.
Pollard, D. D., Segall, P. & Delaney, P. T. 1982. Formation and interpretation of dilatant echelon cracks. *Bull. geol. Soc. Am.* **93**, 1291–1303.
Ritchie, R. O., McClintock, F. A., Nayeb-Hashemi, H. & Ritter, M. A. 1982. Mode III fatigue crack propagation in low alloy steel. *Met. Trans.* **13A**, 101–110.
Rooke, D. P. & Cartwright, D. J. 1976. *Compendium of Stress Intensity Factors.* Procurement Executive, Ministry of Defence, HMSO, London.
Scholz, C. H. 1987. Wear and gouge formation in brittle faulting. *Geology* **15**, 493–495.
Scholz, C. H., Boitnott, G. A. & Nemat-Nasser, S. 1986. The Bridgman ring paradox revisited. *Pure Appl. Geophys.* **124**, 587–599.
Segall, P. & Pollard, D. D. 1980. Mechanics of discontinuous faults. *J. geophys. Res.* **85**, 4337–4350.
Segall, P. & Pollard, D. D. 1983. Nucleation and growth of strike slip faults in granite. *J. geophys. Res.* **88**, 555–568.
Segall, P. & Simpson, C. 1986. Nucleation of ductile shear zones on dilatant fractures. *Geology* **14**, 56–59.
Shamina, O. G., Pavlov, A. A., Strizhkov, S. A. & Kopnichev, Yu. F. 1975. Ultrasonic sounding of region of preparation of solitary macrocrack. In: *Physics of the Earthquake Focus* (edited by Sadovskii, M. A.) Nauka, Moscow, 92–119. English translation published by Amerind, New Delhi, India, 1985.
Sharp, R. V. 1979. Implications of surficial strike-slip fault patterns for simplification and widening with depth. In *Proc. Conf. VIII—Analysis of actual fault-zones in bed rock.* USGS Open File Report No. 79-1239, 66–78.
Sobolev, G. A. 1986. The study of barrier fracture in relation to earthquake and rockburst prediction. *Pure Appl. Geophys* **124**, 811–824.
Sobolev, G. A. & Shamina, O. G. 1975. Present position of laboratory studies of fracture processes as applied to physics of earthquake. In: *Physics of the earthquake focus* (edited by Sadovskii, M. A.) . Nauka, Moscow, 67–91. English translation published by Amerind, New Delhi, India, 1985.
Swanson, P. L. 1984. Subcritical crack growth and other time- and environment-dependent behavior in crustal rocks. *J. geophys. Res.* **89**, 4137–4152.
Swanson, P. L. 1987. Tensile fracture resistance mechanisms in brittle polycrystals: and ultrasonics and *in situ* microscopy investigation. *J. geophys. Res.* **92**, 8015–8036.
Tada, H., Paris, P. C. & Irwin, G. C. 1973. *The Stress Analysis of Cracks Handbook.* Del Research Corp, Hellertown, Pennsylvania.
Tapponnier, P. & Brace, W. F. 1976. Development of stress-induced microcracks in Westerly granite. *Int. J. Rock Mech. Min. Sci. Geomech. Abs.* **13**, 103–112.
Wallace, R. E. & Morris, H. T. 1986. Characteristics of faults and shear zones in deep mines. *Pure Appl. Geophys.* **124**, 107–125.
Wawersik, W. R. & Brace, W. F. 1971. Post failure behavior of a granite and a diabase. *Rock Mech.* **3**, 61–85.
Wong, T-f. 1982. Micromechanics of faulting in Westerly granite. *Int. J. Rock Mech. Min. Sci. Geomech. Abs.* **19**, 49–64.
Wong, T-f. & Biegel, R. 1985. Effects on pressure on the micromechanics of faulting in San Marcos gabbro. *J. Struct. Geol.* **7**, 737–749.

APPENDIX

Materials used

Two contrasting rock types were used in this study. Solnhofen limestone is an ultrafine-grained (max 2 μm) micritic limestone. It is uniform except for thin (< 1 mm) irregularly spaced (5–30 mm) finer grained layers parallel to bedding. The cores were cut with axes parallel to bedding. Westerly granite is a uniform, fine-grained (0.1–1 mm) pink granite with composition approximately 30% quartz, 35% orthoclase, 30% plagioclase feldspars and 5% biotite. The block from which the samples were cut has no petrographic fabric, but a weak microcrack fabric defines the 'rift' plane. All cores were cut parallel and with the rift plane along the axis. The samples had a diameter of 34.8 mm and the slot was cut with a diamond saw with thickness 0.4 mm to a depth of between 5 and 8.6 mm.

Experimental details

Loading was servo-controlled with tangential displacements (twist) as feedback making the machine very stiff in this loading mode. The samples were deformed by imposing a series of twist offsets, after each of which the torque was observed to relax until it reached an equilibrium level, in the range 30–100 Nm. Thus, shear deformation was mainly achieved under load relaxation, producing dominantly quasi-static behavior.

Some deformation experiments were terminated when sharp drops in the load supported were observed. In all cases abrupt load drops were found to correlate with spiral or axial fractures when the samples were sectioned.

Preparation of sections

Deformed specimens were removed carefully from the loading apparatus while supported by a cradle employing the mounts of the displacement transducer used for the mechanical experiments. A low-viscosity epoxy was injected into the notch and allowed to cure before the sample was removed from the cradle. In this way we are confident that no extra damage was introduced in the specimen after the termination of the controlled loading and before sections were prepared. The central section was removed using high-speed, very low feed-pressure, parallel diamond saws, then sections cut parallel to the specimen axis using a low-speed gravity feed thin (0.5 mm) diamond saw (Fig. 2a). After the initial cut, subsequent thick sections (0.2–1 mm) were supported by an aluminum plate glued to the surface with epoxy cement. The low-speed saw was used to minimize near surface damage in the sections. The cut faces were hand lapped successively with 20, 5 and 0.3 μm Al_2O_3 polishing compounds, and finally cleaned in water in an ultrasonic bath to remove polishing residue. At the magnifications used here, iron milling was not required.

We found that the reflectivity contrast between the polished surfaces and the emerging cracks allowed us to easily identify cracks in the granite. Cracks in the limestone showed up in two ways: (1) open cracks, sometimes filled with epoxy, gave a reflectivity contrast similar to the granite; (2) fine damage zones, with little visible offset, appeared as white lines, apparently of finer grain size material, against the cream-colored background.

These could all be seen with the unaided eye by orienting the sample carefully. However, the latter proved particularly demanding to photograph clearly, and generally getting reflected light microscopic images with sufficient contrast presented some problems. Bright field illumination provided the best image from reflectivity contrast, but an oblique specimen surface angle was required, which led to focusing difficulties over the large field depth. Also, in photographs, the high contrast led to reduced definition of the crack morphology.

After examination under reflected light, some of the sections were then cleaned again and prepared for the scanning electron microscope by coating with a gold–palladium film. The scale of the features being studied meant that the very lowest magnifications had to be used. The advantage of using a back-scattered electron image from the S.E.M. is that its primary image is of topography, which is the way in which the cracks are manifested on an otherwise smooth polished surface. Particularly good images were obtained again for the granite, though for the limestone, some of the closed damage zones that could be seen in reflected light could not be so easily detected with the S.E.M.